Polypyrrole Coated Mn–Fe Bimetallic Oxides as High Stability Anode for Lithium-ion Batteries

Yuan Fang
Shaanxi University of Science and Technology Xi\'an Campus: Shaanxi University of Science and Technology

Tengfei Li
Shaanxi University of Science and Technology Xi\'an Campus: Shaanxi University of Science and Technology

Fen Wang (wangf@sust.edu.cn)
Shaanxi University of Science and Technology Xi\'an Campus: Shaanxi University of Science and Technology https://orcid.org/0000-0003-1035-2205

Jianfeng Zhu
Shaanxi University of Science and Technology Xi\'an Campus: Shaanxi University of Science and Technology

Research Article

Keywords: Lithium-ion batteries, High stability anode, Electrochemical performance, Transition metal oxides, Polypyrrole

Posted Date: February 23rd, 2021

DOI: https://doi.org/10.21203/rs.3.rs-223472/v1

Title: Polypyrrole Coated Mn–Fe Bimetallic Oxides as High Stability Anode for Lithium-ion Batteries

Authors: Yuan Fang, Tengfei Li, Fen Wang and Jianfeng Zhu

Corresponding author: Fen Wang (wangf@sust.edu.cn)

Institution: School of Materials Science Engineering, Shaanxi University of Science and Technology; Shaanxi Key Laboratory of Green Preparation and Functionalization for Inorganic Materials, Xi'an 710021, PR China

Abstract: Transition metal oxides as anode materials have received extensive research owing to the high specific capacity. Whereas, the rapid decline of battery capacity caused by volume expansion and low electrical conductivity hinders the practical application of transition metal oxides. This study reported a pseudo-capacitance material polypyrrole coated Fe_2O_3/Mn_2O_3 composites material as a high stability anode for lithium-ion batteries. The polypyrrole coating layer can not only serve as a conductive network to improve electrode conductivity but also can be used as a protective buffer layer to suppress the volume change of Fe_2O_3/Mn_2O_3 during the charging and discharging process. At the same time, the porous structure of Fe_2O_3/Mn_2O_3 composite can not only provide more active sites for lithium storage but also play a certain buffer effect on the volume change of the material. Polypyrrole-coated Fe_2O_3/Mn_2O_3 composite as the anode for lithium-ion batteries shows great electrochemical storage performance, with high specific capacity (627 mAh g^{-1} at a current density of 1A g^{-1}), great cycle stability (the capacity not shows obvious signs of attenuation after 500 cycles) and rate performance (432 mAh g^{-1} at a current density of 2.0 A g^{-1}).

Keywords: Lithium-ion batteries; High stability anode; Electrochemical performance; Transition metal oxides; Polypyrrole

Conflicts of interest: The authors declare that they have no competing interests

Polypyrrole Coated Mn–Fe Bimetallic Oxides as High Stability Anode for Lithium-ion Batteries

Yuan Fang, Tengfei Li, Fen Wang* and Jianfeng Zhu

School of Materials Science Engineering, Shaanxi University of Science and Technology; Shaanxi Key Laboratory of Green Preparation and Functionalization for Inorganic Materials, Xi'an 710021, PR China

* Corresponding author: wangf@sust.edu.cn

Abstract: Transition metal oxides as anode materials have received extensive research owing to the high specific capacity. Whereas, the rapid decline of battery capacity caused by volume expansion and low electrical conductivity hinders the practical application of transition metal oxides. This study reported a pseudo-capacitance material polypyrrole coated Fe_2O_3/Mn_2O_3 composites material as a high stability anode for lithium-ion batteries. The polypyrrole coating layer can not only serve as a conductive network to improve electrode conductivity but also can be used as a protective buffer layer to suppress the volume change of Fe_2O_3/Mn_2O_3 during the charging and discharging process. At the same time, the porous structure of Fe_2O_3/Mn_2O_3 composite can not only provide more active sites for lithium storage but also play a certain buffer effect on the volume change of the material. Polypyrrole-coated Fe_2O_3/Mn_2O_3 composite as the anode for lithium-ion batteries shows great electrochemical storage performance, with high specific capacity (627 mAh g^{-1} at a current density of 1A g^{-1}), great cycle stability (the capacity not shows obvious signs of attenuation after 500 cycles) and rate performance (432 mAh g^{-1} at a current density of 2.0 A g^{-1}).

Keywords: Lithium-ion batteries; High stability anode; Electrochemical performance; Transition metal oxides; Polypyrrole

1. Introduction:

Lithium-ion batteries (LIBs) have become the primary electrochemical energy storage devices due to high energy density and excellent cycling stability. However,

with the continuous development of battery technology, its energy density requirements are getting higher and higher. The traditional anode material graphite has been unable to meet the rapid development of LIBs due to its relatively low specific capacity (372 mAh g^{-1}).[1-3] Therefore, the development of a new generation of great performance anode materials with high energy density and cycle stability is an inevitable trend for the development of LIBs.

In recent years, transition metal oxides, with high theoretical specific capacity and low cost, have received widespread attention as a promising anode candidate for LIBs [4, 5]. Additionally, the transition metal oxides as anode materials have a high lithium insertion potential, which can effectively prevent the accumulation of lithium metal form forming lithium branch crystals when the battery is overcharged, thereby improving the safety performance of LIBs[6]. Among them, Mn_2O_3 and Fe_2O_3 are considered as one of the ideal anode materials by reason of the higher theoretical capacity (1018 and 1007 mAh g^{-1}, respectively) and abundant resource reserves. Mn_2O_3 and Fe_2O_3 bimetal oxides have a large number of heterojunction interfaces, and the existence of heterojunction interfaces and the synergistic effect between the interfaces can also effectively promote the oxidation-reduction reaction[7]. However, owing to the poor electronic conductivity and a large amount of volume expansion during the charge/discharge cycling, the battery capacity will decrease rapidly, and the rate performance will be poor, which limits its practical application[3]. In view of the above problems, the composite method of nano-porous transition metal oxides, carbon nanotubes, and graphene materials were be designed to alleviate the volume expansion of oxides during the cycling and improve the conductivity[8-11]. For example, manganese oxide/graphene and manganese oxide/carbon nanotubes have been successfully prepared [12, 13], and have shown good electrochemical performance. Whereas, in the preparation process of most graphene composite materials, highly toxic hydrazine hydrate is used as a reducing agent, and the prices of graphene and carbon nanotubes are relatively high, which will further increase the production cost of the material. Polypyrrole (PPy), as a pseudo-capacitance material for supercapacitors, has the advantages of high conductivity, good flexibility, simple production, and low price.

This pseudo-capacitance material can store charge on the electrode material surface, so compared with batteries, the electrode is less degraded and has better cycle stability. Introducing it into the transition metal oxide anode material can effectively improve its electrochemical stability[14, 15]. Studies have found that the interface pseudo-capacitance can increase the storage capacity of lithium[16]. Unlike other metal oxides, manganese oxide's redox reaction occurs in a wide potential range and allows the existence of pseudo-capacitance charge and discharge properties[17]. Therefore, the composite of manganese oxide and this flexible polymer conductive material is an important method to improve its electrochemical performance.

In this study, PPy-coated Fe_2O_3/Mn_2O_3 composite was successfully synthesized by the hydrothermal method and the in-situ polymerization (SIP) method, and the effect of polypyrrole on the electrochemical performance of Fe_2O_3/Mn_2O_3 was studied. The research results have certain guiding significance for the preparation of high specific capacity, high cycling stability lithium-ion battery anode materials

2. Experimental

2.1 Material synthesis and preparation

All of the reagents used in this experiment are analytical reagents. $MnSO_4 \cdot H_2O$, Fe $(NO_3)_3 \cdot 9H_2O$, urea, ammonium sulfate, P-toluene sulfonic acid, and pyrrole were bought from Sinopharm Chemical Reagent Co., Ltd. Polyvinylidene fluoride, acetylene black, and N-methyl pyrrolidone was provided by Tianjin Comio Chemical Reagent Co., Ltd.

2.1.1 The synthesis of Fe_2O_3/Mn_2O_3 composites

Fe_2O_3/Mn_2O_3 composite material with a porous structure was successfully prepared by two steps of the hydrothermal method and annealing. Firstly, 8 mmol $MnSO_4 \cdot H_2O$ and 4 mmol $Fe(NO_3)_3 \cdot 9H_2O$ were dissolved in 50 ml ultrapure water and magnetically stirred for 30 minutes. Then add 0.4 g Tween-80 and 1.8 g urea and stir until the solution is clear. Then the solution was poured into a 100 ml Teflon-lined stainless-steel reactor and kept at 120 °C for 10 hours. Then the product was washed several times with ethanol and deionized water until the solution is neutral, and the precursor was obtained by drying the product at 60°C. Then the precursor was kept at

800 °C for 5 hours and then cooled with the furnace to obtain a porous structure Fe_2O_3/Mn_2O_3 (MnFeO) composite material.

2.1.2 Synthesis of Fe_2O_3/Mn_2O_3@PPy

Fe_2O_3/Mn_2O_3@PPy composite material was prepared by SIP method. First, 0.3 g of Fe_2O_3/Mn_2O_3 was ultrasonically dispersed in a solution containing P-toluene sulfonic acid (15 mmol) and ammonium sulfate (9 mmol) in 50 ml ultrapure water. Subsequently, the pyrrole solution was then added drop by drop to the suspension and continuously stirred in ice water for 1 hour for further polymerization. The reaction product was dried at 60℃ for 12 h to obtain MnFeO@PPy composite material. For comparison, MnFeO@PPy samples with 5, 10, and 20 uL of pyrrole solution were prepared according to the above steps, and they were denoted as MnFeO@PPy5, MnFeO@PPy10, and MnFeO@PPy20.

2.2 Material characterizations

The phase structure of the samples was investigated by X-ray diffractometer with Cu-Ka radiation (XRD, D/Max 2200PC, Japan). The Fourier infrared spectrum of the sample was measured on Bruker's infrared spectrometer (Vertex70) and passed FESEM (Hitachi S-4800, Japan) and TEM (Tecnai G2 F20, FEI company) to characterize the micromorphology and structure of the sample.

2.3 Electrochemical test

The electrochemical performance of the MnFeO@PPy electrode was characterized by the CR2032 half-cell. The preparation method of the half-cell is as follows: First, the active material, acetylene black and polyvinylidene fluoride binder were uniformly mixed together at a ratio of 5:4:1(w/w), and an appropriate amount of N-methyl pyrrolidone was added to prepare the electrode slurry. It is then evenly coated on copper foil to prepare the working electrode. Then place the negative electrode shell, shrapnel, gasket, lithium sheet, electrolyte, diaphragm, electrolyte, MnFeO@PPy electrode, and positive electrode shell in the order, and then press and seal with a sealing machine. The electrolyte is 1 M LiPF6 solution (using a volume ratio of 1:1:1 solvent mixture of ethylene carbonate, diethyl carbonate, and methyl vinyl carbonate as electrolyte). Cyclic voltammetry (CV) curves with various scanning rates and

electrochemical impedance spectroscopy of the battery were characterized by Koster electrochemical workstation (CS350H). The galvanostatic charge-discharge performance and rate performance of the battery were tested on NEWARE test equipment (CT-4008T).

3. Results and discussion

The phase structure of MnFeO, MnFeO@PPy5, MnFeO@PPy10, MnFeO@PPy20, and pure phase PPy are showing in Fig. 1a. The diffraction peaks of MnFeO, MnFeO@PPy5, MnFeO@PPy10, and MnFeO@PPy20 correspond with Fe_2O_3 (JCPDS No. 99-0060) and Mn_2O_3 (JCPDS No. 89-4836) in the standard card. There are no obvious impurity peaks in the diffraction pattern, which indicates that the prepared sample has a higher purity. The XRD pattern of the pure phase PPy is also shown in Fig. 1a, and there is a clear C peak at about 26°, which is consistent with the literature report[18, 19]. In order to further prove the existence of PPy in the composite material, the sample was tested by FTIR, and the result is shown in Fig. 1b. The peaks at 524 and 570 cm^{-1} correspond to the characteristic peaks of the Fe-O bond and Mn-O bond, respectively[20, 21]. The peaks at 1554 and 1463 cm^{-1} are corresponding to the characteristic peaks of the pyrrole ring; The bands at 1180, 1105, 1045, and 914 cm^{-1} are the characteristic peaks of N-H, C-N-C, C-H, and C-C.[22-24]

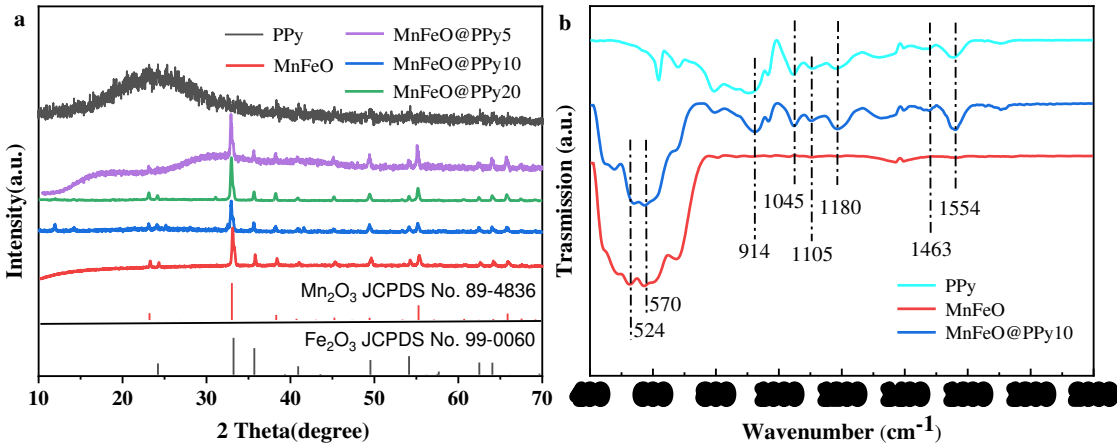

Fig. 1 (a) XRD patterns of MnFeO, MnFeO@PPy5, MnFeO@PPy10, MnFeO@PPy20; (b) Fourier infrared spectra of PPy, MnFeO and MnFeO@PPy10.

The microscopic morphology of the sample was characterized by FESEM, and the result (Fig. 2). Fig. 2a and 2d show the MnFeO microscopic morphologies, it can be

seen that there are showing a porous structure. This channel structure can establish a channel for the rapid transport of lithium ions, and it can effectively alleviate the volume expansion of the active material during charge and discharge, thereby improving the cycle stability of the material. Fig. 2b and 2e are the microscopic morphology of MnFeO@PPy10. It can be seen that unlike MnFeO, the surface of MnFeO@PPy10 has a layer of PPy film. Its high conductivity and good flexibility can further improve its electrical conductivity and stability of chemical properties. The microstructure of MnFeO@PPy10 was further studied by TEM (Fig. 2c, f). It can be seen from Fig. 2c that MnFeO@PPy10 has an obvious porous structure. In the TEM image shown in Fig. 2f, it can be seen that there is a clear PPy coating layer at the boundary of the MnFeO matrix, with a thickness of about 23 nm. The conductive polymer film can further improve the conductivity of MnFeO composite, and the existence of the coating layer can effectively reduce the large volume expansion during the charge and discharge process, and prevent the material structure from being damaged and losing activity.

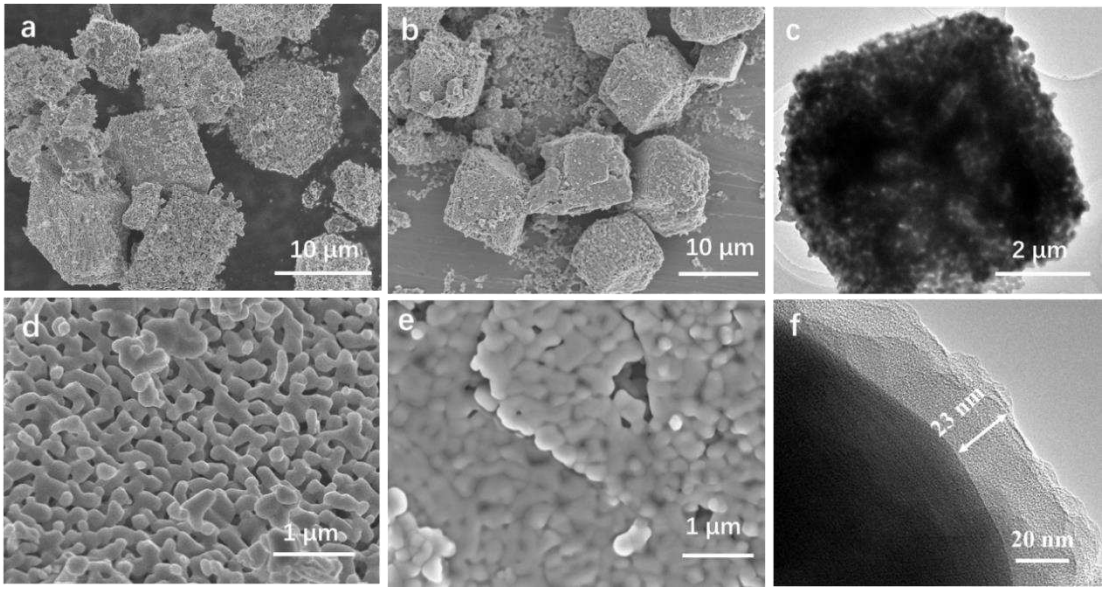

Fig. 2 FESEM images of (a, d) MnFeO and (c, d) MnFeO@PPy10, (e, f) TEM images of MnFeO@PPy10

To characterize the electrochemical reaction kinetics and reversibility of the composites, CV tests were carried out on the battery with MnFeo@PPy10 and MnFeO as the anode at the scanning rate of 0.1mV s^{-1}. The test results are shown in Fig. 3a and

3b. At the first cathodic scanning process of MnFeO@PPy10, three obvious reduction peaks were observed at 0.35 V, 0.95 V, and 1.1 V respectively. The sharp peaks at 0.35 V, 0.95 V are corresponding to Mn(III) → Mn(0) and Fe(III) → Fe(0) respectively. The peak at 1.1 V results from the process of solid electrolyte film-forming by the irreversible reduction reaction of the electrolyte. At the next cathodic scanning test, the reduction peak at 1.1 V disappeared, which further indicates that the solid electrolyte film is an irreversible phase transition. Two obvious oxidation peaks appeared during the anode scanning test. The oxidation peak at 1.31 V was attributed to the reversible oxidation of Fe (0) →Fe (II) and Mn (0) →Mn (II). The oxidation at 1.67 V The formation of the peak is attributed to the reversible oxidation of Fe (II)→Fe (III) and Mn (II)→Mn (III) [25-27]. These two groups of redox peaks did not change significantly in the subsequent tests, and the peak positions basically overlapped, indicating that the electrochemical reaction has good reversibility. Different from MnFeO, the two reduction peaks of MnFeO@PPy10 show a certain left shift in the subsequent cycle test. This is because the introduction of pseudo-capacitance material polypyrrole can store a large amount of charge on the surface of the material during charging. In this process, these stored charges can further reduce the reaction energy barrier and promote the reduction reaction[28].

Fig. 3c and Fig. 3d show the first three charging/discharging curves of MnFeO@PPy10 and MnFeO electrodes at a current density of 0.1 A g^{-1}. It can be seen from Fig. 3c and Fig. 3d that there are three obvious discharge platforms in both MnFeO@PPy10 and MnFeO electrodes during the first discharge (platform 1: 1.1 V; platform 2: 0.9 V; platform 3: 0.3 V). These three platforms correspond to the formation of solid electrolyte membranes, the reduction of Fe(III)→Fe(0), and the reduction of Mn(III)→Mn(0). Among them, platform 1 corresponds to irreversible capacity, and platforms 2 and 3 are reversible capacity. The existence of irreversible capacity determines the size of the first coulombic efficiency[29, 30]. The first charge-discharge specific capacity of MnFeO@PPy10 composite is 995 and 1551 mAh g^{-1}, respectively. The first coulombic efficiency is 64%, which is caused by the irreversible electrochemical reaction and the decomposition of the electrolyte. It has been consistent

with the CV curve analysis.

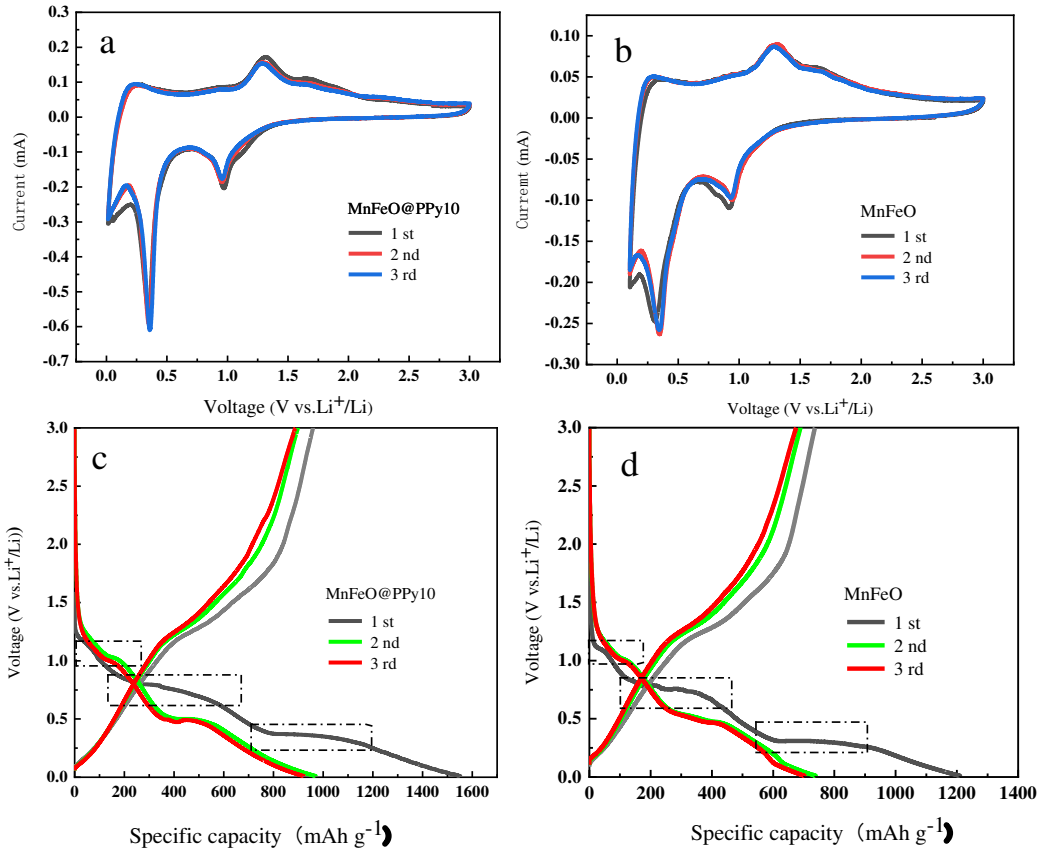

Fig. 3 (a, b) Cyclic voltammogram curves of MnFeO@PPy10 and MnFeO at the scan rate of 0.1 mV s^{-1}; (c, d) The first three charges/discharges curves of MnFeO@PPy10 and MnFeO at 0.1 A g^{-1}.

The cycling performance curves of MnFeO, MnFeO@PPy5, MnFeO@PPy10, and MnFeO@PPy20 electrode materials were characterized by galvanostatic charge/discharge tests at 1 A g^{-1}, and the results are shown in Fig. 4a. The initial charge-discharge specific capacity of the MnFeO electrode reaches 661/1100 mAh g^{-1}, and its capacity loss is mainly caused by the formation of solid electrolyte film by an irreversible electrochemical reaction, which is consistent with CV curve analysis. The battery capacity dropped sharply after 250 cycles of charge and discharge, and after 500 cycles, its capacity dropped to 230 mAh g^{-1}. Unlike MnFeO electrodes, MnFeO@PPy5, MnFeO@PPy10, and MnFeO@PPy20 electrode materials did not show obvious signs of capacity degradation after 500 cycles. After 500 cycles, the specific capacity ratio was 473,628,492 mAh. g^{-1}. The average lithium storage capacities of MnFeO@PPy5, MnFeO@PPy10, and MnFeO@PPy20 electrode materials after 500 charge-discharge

cycles were 483,627,619 mAh g^{-1}, respectively, among which MnFeO@PPy10 showed the most stable lithium storage performance. The MnFeO@PPy10 electrode exhibits a certain capacity decay in the first 50 charge and discharge cycles, which is mainly caused by the irreversible structural transformation caused by the partial volume change in the early stage [31-33]. After 50 cycles, its capacity tends to be stable. Its specific capacity has been fluctuating at 617mAh g^{-1} during the discharging process, showing great cycling stability.

The rate performance of MnFeO and MnFeO@PPy10 were investigated at various current densities (0.1, 0.2, 0.5, 1, 2 A g^{-1}), and Fig. 4b shows the test resuls. The average reversible discharge capacity of MnFeO@PPy10 electrode at 0.1, 0.2, 0.5, 1, 2 A g^{-1} reaches 946, 775, 643, 506 and 432 mAh g^{-1}. When the current density increases from 0.1 A g^{-1} to 2 A g^{-1}, its specific capacity loss is 54.3% of the initial capacity. After the current density decreases again (0.5, 0.1 A g^{-1}), the specific capacity also sequentially recovers to 657,881 mAh g^{-1}. Compared with MnFeO electrode (The specific capacity is 660, 535, 490, 401, 257 mAh g^{-1} at the current density of 0.1, 0.2, 0.5, 1, 2 A g^{-1}, and the capacity loss is 61%), MnFeO@PPy10 shows more excellent rate performance, which further illustrates the MnFeO@PPy10. The specific capacity has better stability and reversibility.

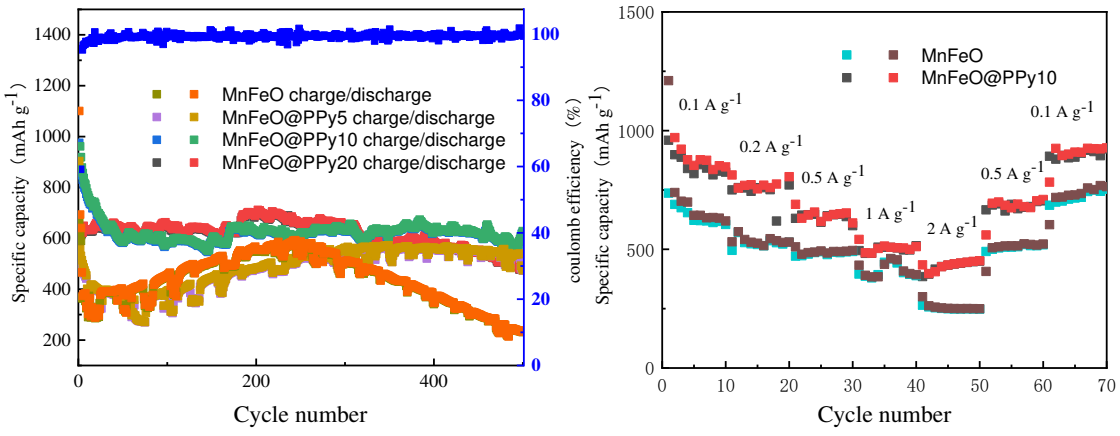

Fig. 4 (a) Cycling performance curves of MnFeO, MnFeO@PPy5, MnFeO@PPy10 and MnFeO@PPy20 at 1 A g^{-1}; (b) Rate performance of MnFeO and MnFeO@PPy10 at different current densities (0.1-2 A g^{-1}).

To further study the capacitance behavior of the MnFeO@PPy10 composite, the

capacitance effect of the MnFeO@PPy10 composite electrode system was analyzed through the CV curves of different scan rates (Fig. 5a). Generally, two charge storage behaviors (capacitive contribution caused by the surface charge transfer and diffusion contribution caused by lithiation/desalination reactions) play an important role in the charge/discharge process. The charge storage process can be characterized by analyzing the relationship between the current response (i) and the scan rate (v). And the capacitance effect of the electrode material can be qualitatively analyzed by the following formulas:

$$i=av^b \tag{1}$$

$$\log i = b \log v + \log a \tag{2}$$

Here a and b are constants. When b is close to 0.5, the electrochemical process is controlled by diffusion, and b is close to 1.0 that the reaction is controlled by the contribution of capacitance. For b values between 0.5 and 1.0, there is a mixing mechanism during charge storage [9, 34]. Fig. 5 b is the fitting curve of $\log i$-$\log v$, calculated from it, the b values of the oxidation peak (peak1, 2) and the reduction peak (peak3, 4) are 0.88, 0.92, 1.0, 0.70 respectively, which indicates that the MnFeO@PPy10 electrode has a good capacitance effect. The proportion of capacitance contribution can be quantitatively calculated by the formula (3), where V is the voltage; i is the corresponding current response; k_1v is the surface capacitance contribution; $k_2v^{1/2}$ contributes to diffusion.

$$i(V)=k_1v+k_2v^{1/2} \tag{3}$$

Fig. 5c shows the capacitance evaluation of the capacitive behavior contribution when the scan rate is 0.1 mV s^{-1}, in which the red shaded part is the capacitive contribution. The capacitive control capacity accounts for 75% of the total charge storage at 0.1 mV s^{-1}. Fig. 5d shows the ratio of the amount of charge stored by the diffusion contribution and the capacitance contribution at various scan rates. The results show that as the scan rate increases from 0.1 to 1 mV s^{-1}, the capacitance contribution of the capacitance behavior increases to 97%. The conductive polymer polypyrrole coating in the MnFeO@PPy10 electrode material can promote the charge transfer of the active material and the capacitance behavior of the MnFeO@PPy10 electrode. This

feature is also conducive to the rapid transport of Li, thereby making its cycle life and reversible capacity stable Enhanced [14].

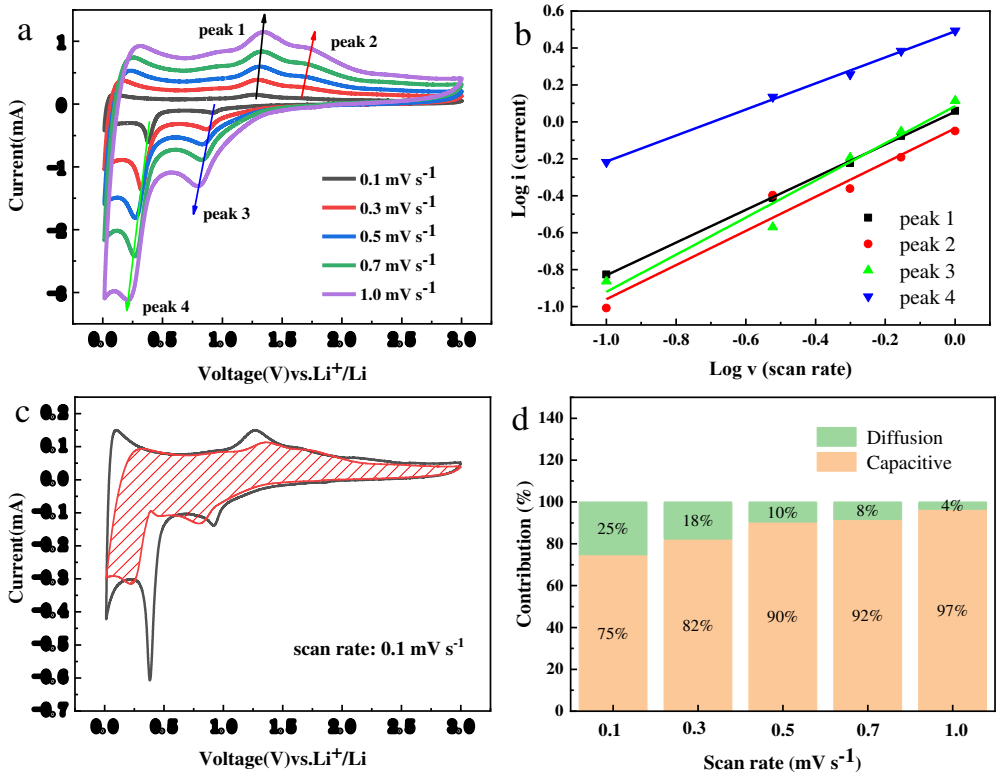

Fig.5 (a) CV curves of MnFeO@PPy10 at different scan rates (0.1-1 mV s^{-1}); (b) Fit curves of Log i versus Log v (i: current; v: scanning rate) at each redox peak; (c) Capacitive (red shaded) and diffusion controlled to charge storage for MnFeO@PPy10 at 0.1 mV s^{-1}. (d) The ratio of capacitive and diffusion contribution at various scan rates.

To investigate the impact of PPy on the conductivity of MnFeO, electrochemical impedance spectroscopy tests were carried out on half-cells with MnFeO and MnFeO@PPy10 as working electrodes. The test results are shown in Fig. 6a. The semicircular area (high frequency) corresponds to the charge transfer process at the electrode/electrolyte interface. The linear part (low frequency), corresponds to the diffusion process of lithium ions in the electrode. The equivalent circuit diagram is shown in the inset of Fig. 6a, where Rs represent the half-cell ohmic impedance; Rf and Rct represent the solid electrolyte film resistance and the surface charge transfer resistance; C1 and C2 represent the phasing elements of the corresponding double-layer capacitors; W1 represents the Warburg impedance caused by the diffusion of lithium ions in the electrode. The impedance value of Rs, Rf and Rct is fitted: MnFeO (Rs=6.4,

Rf=157, Rct=49.3); MnFeO@PPy10 (Rs=5.4, Rf=72.3, Rct=36.9). As shown in Fig. 6b, the resistance of each circuit element is lower than that of the MnFeO electrode. Among them, the resistance of the solid electrolyte membrane and the charge transfer resistance decrease the most. The main reason is that the existence of the pseudo-capacitance material polypyrrole conductive network can store charge in the surface of the electrode material and provides a more convenient channel for electrons and Li^+ to shuttle back and forth during the charging and discharging process. Thereby promoting the charge transfer between the active material, conductive carbon, and the binder, and improving the conductivity of the material. In addition, the porous structure of the MnFeO@PPy10 electrode material can also reduce the aggregation and contact resistance of the electrode, and provide more active sites for the transfer of electrons and ions, thereby promoting the effective progress of the reaction.

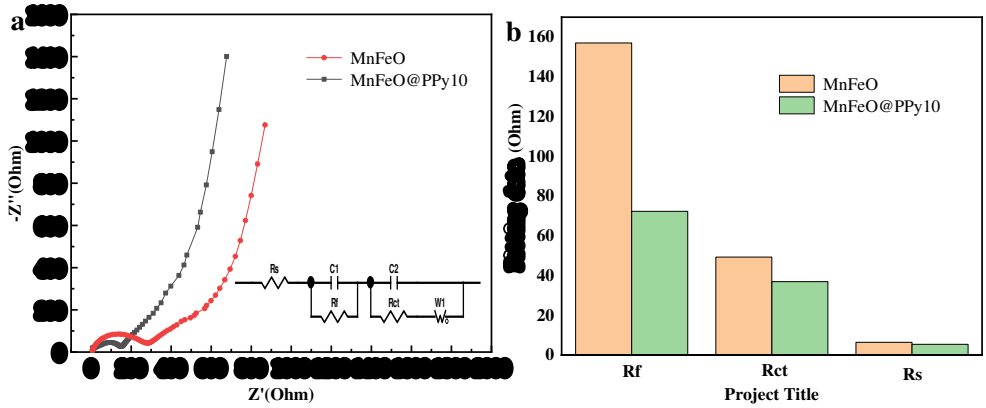

Fig.6 (a) The electrochemical impedance spectra of MnFeO 和 MnFeO@PPy10; (b) Fitting data comparison diagram of each component

3. Conclusion

In this study, MnFeO@PPy10 composite anode material was successfully synthesized through two steps of hydrothermal method and SIP method. The polypyrrole coating layer of pseudo capacitance material has high conductivity and mechanical strength, which can effectively alleviate the volume effect leading to the phenomenon of material inactivation during charging and discharging. The existence of the polypyrrole conductive network can store charges on the surface of the electrode material, which can provide a more convenient channel for electrons and Li^+ to shuttle back and forth during the charging and discharging process. Thereby promoting the

charge transfer between the active material, conductive carbon, and the binder improving the conductivity of the material. The porous structure of Fe_2O_3/Mn_2O_3 is not only conducive to the rapid transmission of Li^+ and electrons but also serves as a volume buffer, thereby improving material stability. Experimental studies show that this pseudo-capacitance polypyrrole coated MnFeO@PPy10 electrode material has good electrochemical performance: higher charge-discharge specific capacity (The specific capacity reaches 627 mAh g^{-1} at 1A g^{-1}), good cycle stability (After 500 cycles, the capacity not shows obvious signs of attenuation), and special rate performance (The specific capacity is 432 mAh g^{-1} at 2.0 A g^{-1}).

Acknowledgments

The authors acknowledge financial support from the National Natural Science Foundation of China (No. 51972201), China Postdoctoral Science Foundation (No. 2019M663607). This work is also supported by the Doctoral Starting up Foundation of Shaanxi University of Science and Technology (No. 2016BJ-75).

Reference

[1] JB Goodenough, Y Kim Chemistry of Materials 22: 587 (2010) https://doi.org/10.1021/cm901452z
[2] L Ji, Z Lin, M Alcoutlabi, X Zhang Energ Environ Sci 4: (2011) https://doi.org/10.1039/c0ee00699h
[3] W Xu, JL Wang, F Ding, et al. Energ Environ Sci 7: 513 (2014) https://doi.org/10.1039/c3ee40795k
[4] L Zhang, L Hou, L Lian, L Wang, C Yuan Rare Metal Materials and Engineering 45: 1910 (2016) https://doi.org/10.1007/s11434-015-0771-6
[5] R Marom, SF Amalraj, N Leifer, D Jacob, D Aurbach Journal of Materials Chemistry 21: 9938 (2011) https://doi.org/10.1039/c0jm04225k
[6] J Zhang, A Yu Science Bulletin 60: 823 (2015) https://doi.org/10.1007/s11434-015-0771-6
[7] Y Fang, Y Wang, F Wang, C Shu, J Zhu, W Wu RSC Advances 8: 8678 (2018) https://doi.org/10.1039/c7ra12610g
[8] J-L Niu, G-X Hao, J Lin, et al. Inorganic Chemistry 56: 9966 (2017) https://doi.org/10.1021/acs.inorgchem.7b01486
[9] C Hou, Z Tai, L Zhao, et al. J Mater Chem A 6: 9723 (2018) https://doi.org/10.1039/c8ta02863j
[10] T Bai, H Zhou, J Yang, J Tang, X Zhou J. Electroanal. Chem. 815: 98 (2018) https://doi.org/10.1016/j.jelechem.2018.02.002
[11] W-M Chen, L Qie, Y Shen, et al. Nano Energy 2: 412 (2013) https://doi.org/10.1016/j.nanoen.2012.11.010
[12] JW Lee, AS Hall, J-D Kim, TE Mallouk Chemistry of Materials 24: 1158 (2012) https://doi.org/10.1021/cm203697w
[13] S Yuan, W Chen, L Zhang, et al. Small: (2019) https://doi.org/10.1002/smll.201903311

[14] J Liu, W Zhou, L Lai, et al. Nano Energy 2: 726 (2013) https://doi.org/10.1016/j.nanoen.2012.12.008
[15] D Luo, N Zhao, J Wu, Y Ni, C Wang, Y Cao Crystal Research and Technology 54: (2019) https://doi.org/10.1002/crat.201900025
[16] Y Chu, L Guo, B Xi, et al. Adv. Mater. 30: (2018) https://doi.org/10.1002/adma.201704244
[17] Q Liu, Y Luo, W Chen, Y Yan, L Xue, W Zhang Chem Eng J 347: 455 (2018) https://doi.org/10.1016/j.cej.2018.04.138
[18] J Guo, H Gu, H Wei, et al. The Journal of Physical Chemistry C 117: 10191 (2013) https://doi.org/10.1021/jp402236n
[19] D Lu, ZJ Yao, YQ Li, et al. J Colloid Interf Sci 565: 218 (2020) https://doi.org/10.1016/j.jcis.2020.01.023
[20] L Feng, Y Zhang, R Wang, et al. Nanoscale Research Letters 12: (2017) https://doi.org/10.1186/s11671-017-2286-3
[21] D Luo, J Wu, Y Ni, C Wang, N Zhao Transactions of the Indian Ceramic Society 78: 34 (2019) https://doi.org/10.1080/0371750x.2019.1583134
[22] F Yin, J Ren, Y Zhang, T Tan, Z Chen Nanoscale Research Letters 13: (2018) https://doi.org/10.1186/s11671-018-2724-x
[23] D-S Liu, D-H Liu, B-H Hou, et al. Electrochim. Acta 264: 292 (2018) https://doi.org/10.1016/j.electacta.2018.01.129
[24] Q Ye, J Ru, J Peng, G Chen, D Wang Chem Eng J 331: 570 (2018) https://doi.org/10.1016/j.cej.2017.09.031
[25] JS Cho, YJ Hong, YC Kang Acs Nano 9: 4026 (2015) https://doi.org/10.1021/acsnano.5b00088
[26] KW Zeng, XH Li, ZX Wang, et al. Electrochim. Acta 247: 795 (2017) https://doi.org/10.1016/j.electacta.2017.07.070
[27] X Zhang, Y Qian, Y Zhu, K Tang Nanoscale 6: 1725 (2014) https://doi.org/10.1039/c3nr05551e
[28] O Delmer, P Balaya, L Kienle, J Maier Zeitschrift für anorganische und allgemeine Chemie 634: 2011 (2008) https://doi.org/10.1002/zaac.200870007
[29] K Zhong, X Xia, B Zhang, H Li, Z Wang, L Chen J. Power Sources 195: 3300 (2010) https://doi.org/10.1016/j.jpowsour.2009.11.133
[30] K Zhong, B Zhang, S Luo, et al. J. Power Sources 196: 6802 (2011) https://doi.org/10.1016/j.jpowsour.2010.10.031
[31] Y Sun, X Hu, W Luo, Y Huang Journal of Materials Chemistry 22: 19190 (2012) https://doi.org/10.1039/c2jm32036c
[32] Q-Z Gou, C Li, X-Q Zhang, et al. Journal of Materials Science: Materials in Electronics 29: 16064 (2018) https://doi.org/10.1007/s10854-018-9695-7
[33] A Ponrouch, P-L Taberna, P Simon, MR Palacín Electrochim. Acta 61: 13 (2012) https://doi.org/10.1016/j.electacta.2011.11.029
[34] J Zhang, W Zhang, T He, et al. Carbon 115: 95 (2017) https://doi.org/10.1016/j.carbon.2016.12.090

Figures

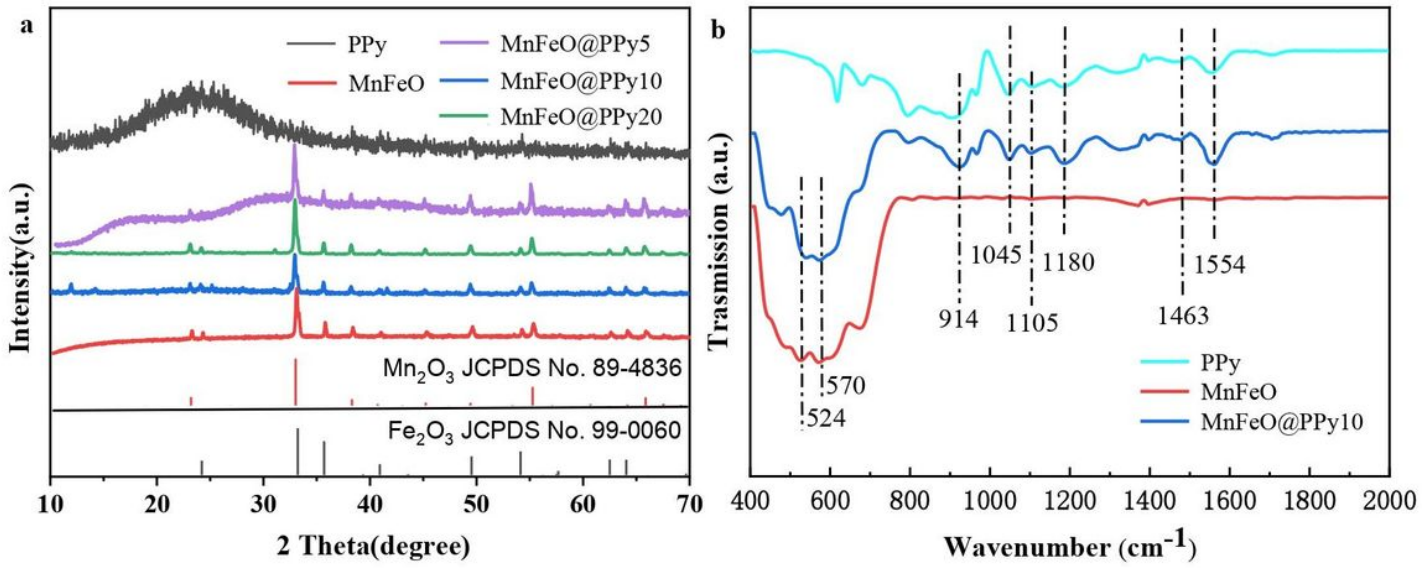

Figure 1

(a) XRD patterns of MnFeO, MnFeO@PPy5, MnFeO@PPy10, MnFeO@PPy20; (b) Fourier infrared spectra of PPy, MnFeO and MnFeO@PPy10.

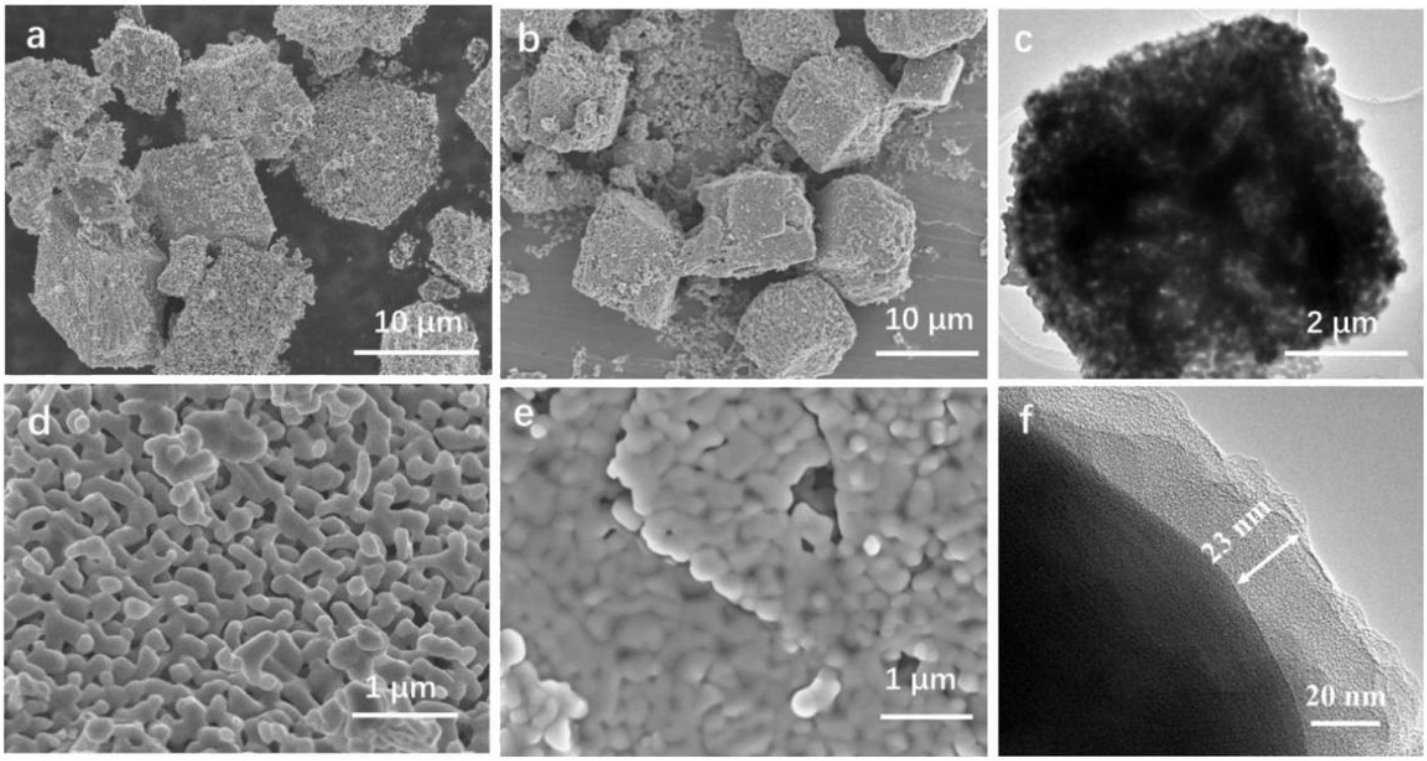

Figure 2

FESEM images of (a, d) MnFeO and (c, d) MnFeO@PPy10, (e, f) TEM images of MnFeO@PPy10

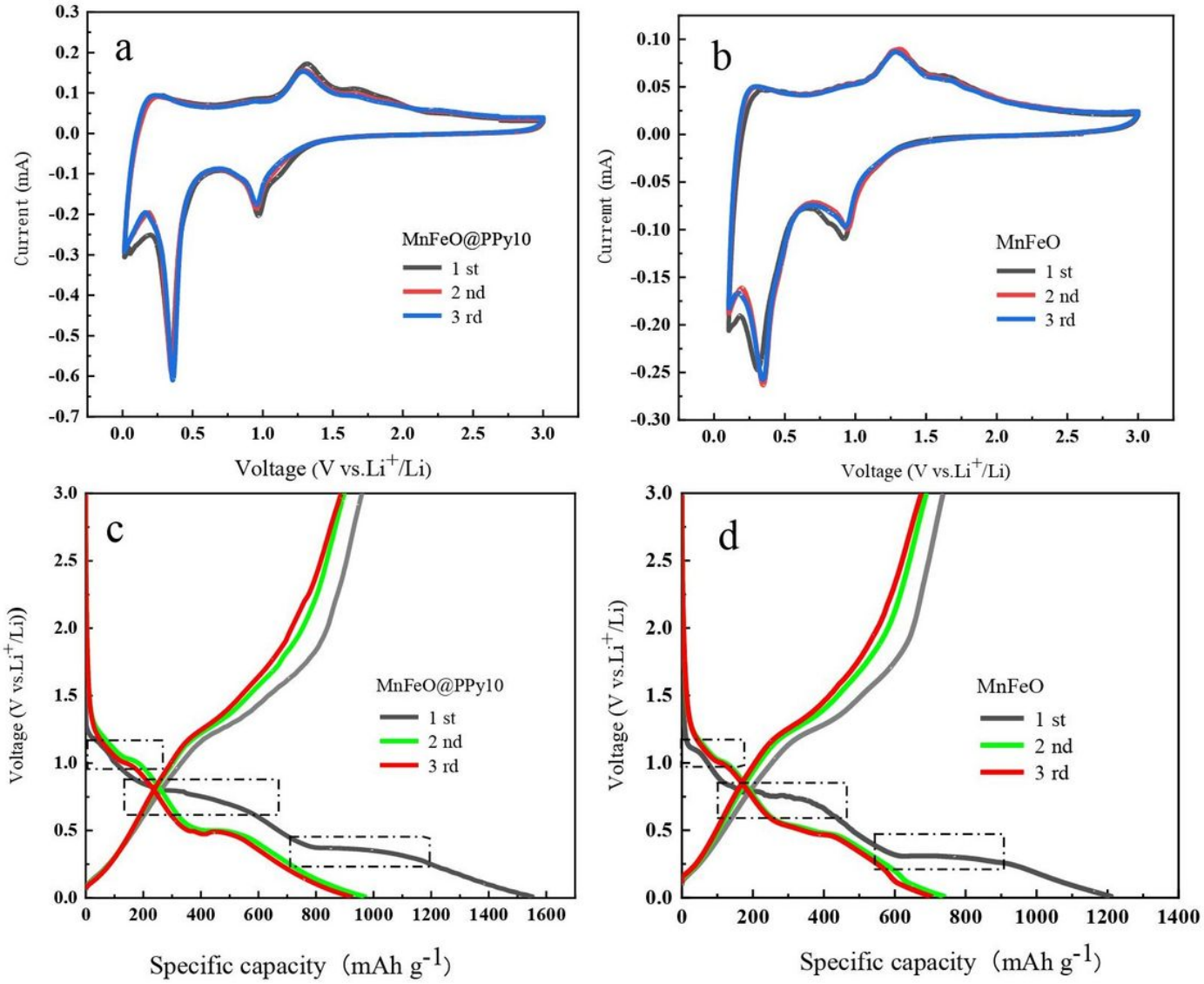

Figure 3

(a, b) Cyclic voltammogram curves of MnFeO@PPy10 and MnFeO at the scan rate of 0.1 mV s-1; (c, d) The first three charges/discharges curves of MnFeO@PPy10 and MnFeO at 0.1 A g-1.

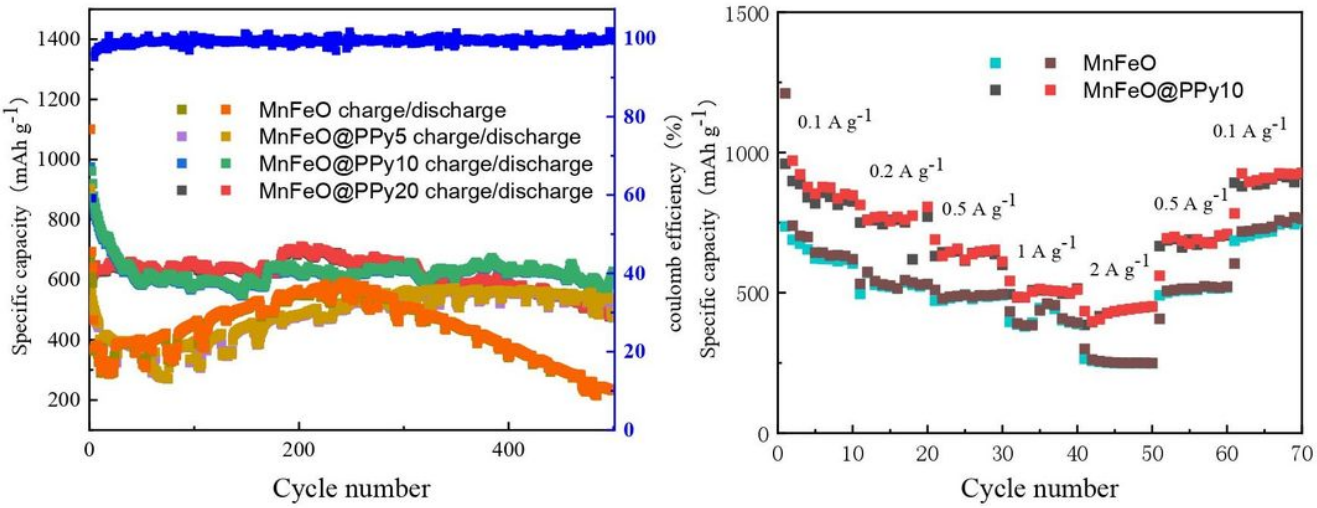

Figure 4

(a) Cycling performance curves of MnFeO, MnFeO@PPy5, MnFeO@PPy10 and MnFeO@PPy20 at 1 A g-1;
(b) Rate performance of MnFeO and MnFeO@PPy10 at different current densities (0.1-2 A g-1).

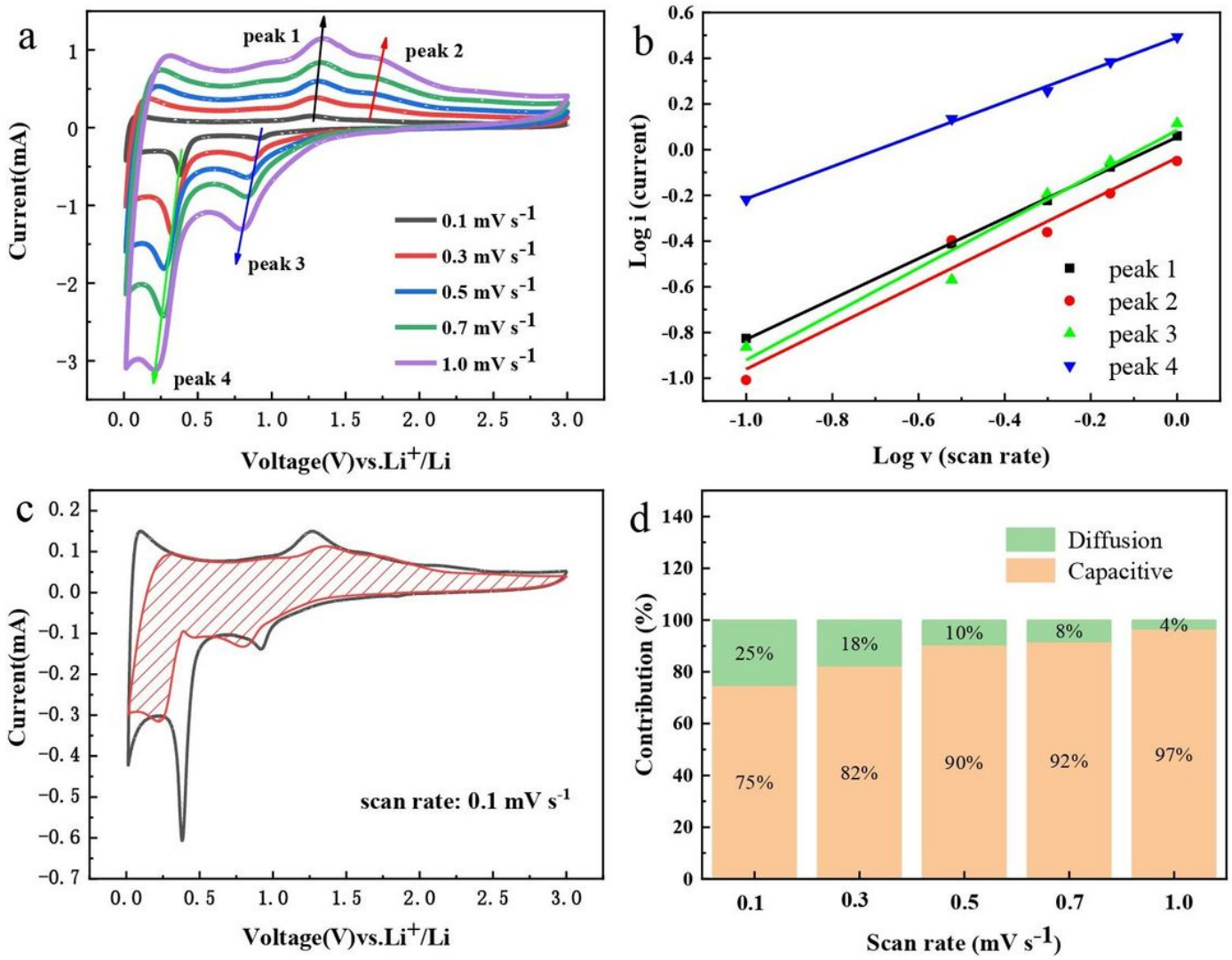

Figure 5

(a) CV curves of MnFeO@PPy10 at different scan rates (0.1-1 mV s-1); (b) Fit curves of Log i versus Log v (i: current; v: scanning rate) at each redox peak; (c) Capacitive (red shaded) and diffusion controlled to charge storage for MnFeO@PPy10 at 0.1 mV s-1. (d) The ratio of capacitive and diffusion contribution at various scan rates.

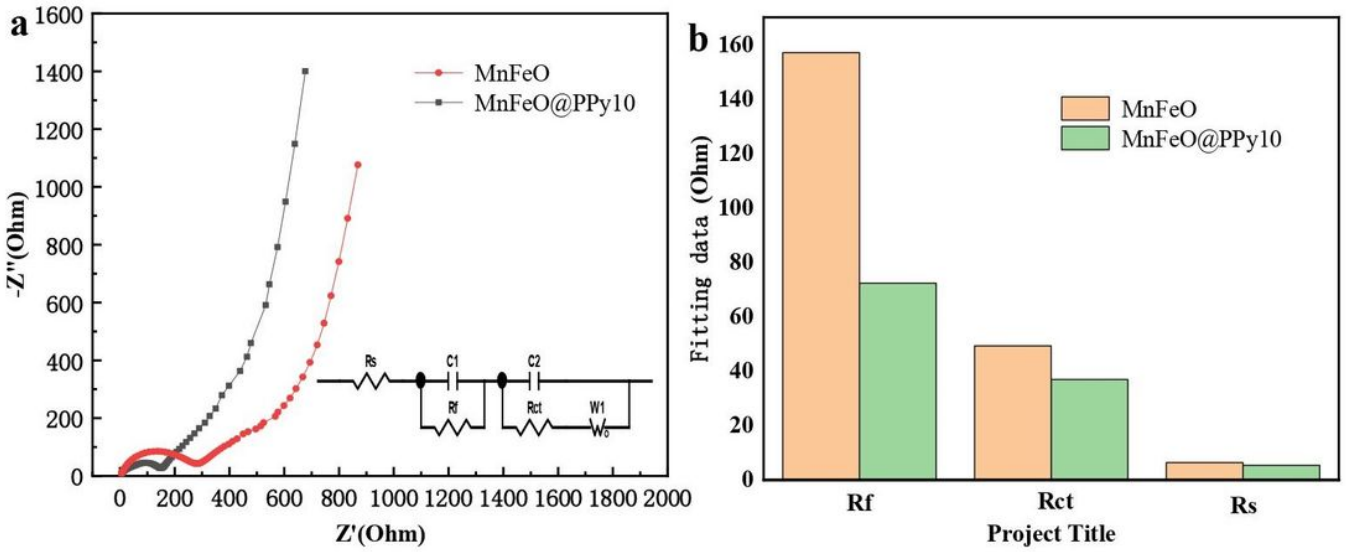

Figure 6

(a) The electrochemical impedance spectra of MnFeO□MnFeO@PPy10; (b) Fitting data comparison diagram of each component